CrossMark
click for updates

Slide-and-exchange mechanism for rapid and selective transport through the nuclear pore complex

Barak Raveh[a,b,c,1], Jerome M. Karp[d,e,1], Samuel Sparks[d,e,1], Kaushik Dutta[f], Michael P. Rout[g], Andrej Sali[a,b,c,2], and David Cowburn[d,e,2]

[a]Department of Bioengineering and Therapeutic Sciences, University of California at San Francisco, San Francisco, CA 94143; [b]Department of Pharmaceutical Chemistry, University of California at San Francisco, San Francisco, CA 94143; [c]California Institute for Quantitative Biosciences, University of California at San Francisco, San Francisco, CA 94143; [d]Department of Biochemistry, Albert Einstein College of Medicine, Bronx, NY 10461; [e]Department of Physiology & Biophysics, Albert Einstein College of Medicine, Bronx, NY 10461; [f]NMR Department, New York Structural Biology Center, New York, NY, 10027; and [g]Laboratory of Cellular and Structural Biology, Rockefeller University, New York, NY 10065

Edited by Michael L. Klein, Temple University, Philadelphia, PA, and approved March 18, 2016 (received for review November 23, 2015)

Nucleocytoplasmic transport is mediated by the interaction of transport factors (TFs) with disordered phenylalanine-glycine (FG) repeats that fill the central channel of the nuclear pore complex (NPC). However, the mechanism by which TFs rapidly diffuse through multiple FG repeats without compromising NPC selectivity is not yet fully understood. In this study, we build on our recent NMR investigations showing that FG repeats are highly dynamic, flexible, and rapidly exchanging among TF interaction sites. We use unbiased long timescale all-atom simulations on the Anton supercomputer, combined with extensive enhanced sampling simulations and NMR experiments, to characterize the thermodynamic and kinetic properties of FG repeats and their interaction with a model transport factor. Both the simulations and experimental data indicate that FG repeats are highly dynamic random coils, lack intrachain interactions, and exhibit significant entropically driven resistance to spatial confinement. We show that the FG motifs reversibly slide in and out of multiple TF interaction sites, transitioning rapidly between a strongly interacting state and a weakly interacting state, rather than undergoing a much slower transition between strongly interacting and completely noninteracting (unbound) states. In the weakly interacting state, FG motifs can be more easily displaced by other competing FG motifs, providing a simple mechanism for rapid exchange of TF/FG motif contacts during transport. This slide-and-exchange mechanism highlights the direct role of the disorder within FG repeats in nucleocytoplasmic transport, and resolves the apparent conflict between the selectivity and speed of transport.

nuclear pore | molecular dynamics | nucleoporins | transport factors | NMR

The nuclear pore complex (NPC) regulates macromolecular transport between the nucleus and the cytoplasm in all eukaryotic cells (1, 2). The NPC allows for passive diffusion of small molecules including sugars, ions, and water, while simultaneously imposing size-dependent exclusion of macromolecules without nuclear transport factor (TF) binding sites, generating unique nuclear and cytoplasmic compartments (3, 4). Larger macromolecules can bypass the selectivity barrier of the NPC by interacting with TFs that shuttle cargo through the central channel of the pore. In pathological conditions, including many cancers and viral infections, the NPC is hijacked and used to transport undesired particles, or it is modified to attenuate the cellular responses to disease onset (5, 6).

TFs traverse the NPC by selective and reversible association with disordered phenylalanine-glycine (FG) repeat domains of the FG nucleoporin proteins (FG Nups), which line the surface of the NPC (7–14). Each FG repeat domain consists of 5–50 FG repeats. In turn, each FG repeat consists of a single FG motif of various sequence flavors, such as the FSFG and GLFG motifs, and 10–30 spacer residues that separate consecutive FG motifs (15, 16). The spacer residues are strongly hydrophilic (17) and rich in disorder-promoting residues, such as proline, serine, lysine, and glutamine (Fig. 1) (18). Each NPC contains thousands of individual FG motifs that function as potential interaction sites for TFs during transport (19, 20).

A key question is how TFs transport rapidly through the FG repeats, with measured dwell times of approximately milliseconds (21, 22), while interacting sufficiently strongly with the FG repeats to maintain a high level of transport selectivity. Several proposed models of NPC transport differ significantly with regard to assumptions about the structure and dynamics of the FG repeats, their interactions with each other and with TFs, and their structural changes during these interactions (1, 3, 15, 23–28). For instance, in the hydrogel model, a dense meshwork of FG Nups forms a conformationally restrained hydrogel that is dissolved locally by the passage of TFs through the nuclear pore. In the virtual gate/polymer brush model, diffuse and dynamic FG Nups create an entropic barrier that prevents nonspecific transport, but is overcome by interaction with TFs. To describe the free energy landscape of the transport system more accurately and precisely, we need additional high-resolution structural, thermodynamic, and kinetic information.

Prior work from our group, using detailed NMR studies, revealed that FG repeats undergo rapid dynamic exchange at multiple low-affinity interaction sites on TF surfaces, and showed that they remain highly disordered while transiently interacting

Significance

The nuclear pore complex (NPC) mediates the trafficking of macromolecules in and out of the nucleus of eukaryotic cells. Here, we characterize how transport factors diffuse rapidly through multiple layers of disordered phenylalanine-glycine (FG) repeat domains lining the NPC. Transport factors interact with FG repeats through a dynamic sliding motion, enabling faster translocation through the NPC than that attainable by a two-state binding mechanism as well as effectively blocking the passage of large macromolecules that do not bind to transport factors. Thus, the NPC exemplifies a dynamic system in living cells, the function of which depends on protein–protein interactions that are transient on the one hand, and highly specific on the other.

Author contributions: B.R., J.M.K., S.S., A.S., and D.C. designed research; B.R., J.M.K., S.S., K.D., and D.C. performed research; B.R., M.P.R., A.S., and D.C. contributed new reagents/analytic tools; B.R., J.M.K., S.S., K.D., and D.C. analyzed data; and B.R., J.M.K., S.S., K.D., M.P.R., A.S., and D.C. wrote the paper.

The authors declare no conflict of interest.

This article is a PNAS Direct Submission.

Data deposition: Simulations and scripts have been deposited at https://github.com/integrativemodeling/npc_slide_and_exchange.

[1]B.R., J.M.K., and S.S. contributed equally to this work.

[2]To whom correspondence may be addressed. Email: david.cowburn@einstein.yu.edu or sali@salilab.org.

This article contains supporting information online at www.pnas.org/lookup/suppl/doi:10.1073/pnas.1522663113/-/DCSupplemental.

BIOPHYSICS AND COMPUTATIONAL BIOLOGY
APPLIED PHYSICAL SCIENCES
Downloaded by guest on February 24, 2022

A

$FSFG_6$	$FSFG_2$
MDNKTTNTTPS	MAKPAEKNNNETSKPA
FSFGAKSDENKAGATSKPA	**FSFG**AKSDDEKKGDASKPA
FSFGAKPEEKKDDNSSKPA	**FSFG**AKPDENKASATSKPA
FSFGAKSNEDKQDGTAKPA	
FSFGAKPAEKNNNETSKPA	
FSFGAKSDDEKKGDASKPA	
FSFGAKPDENKASATSKPA	

B

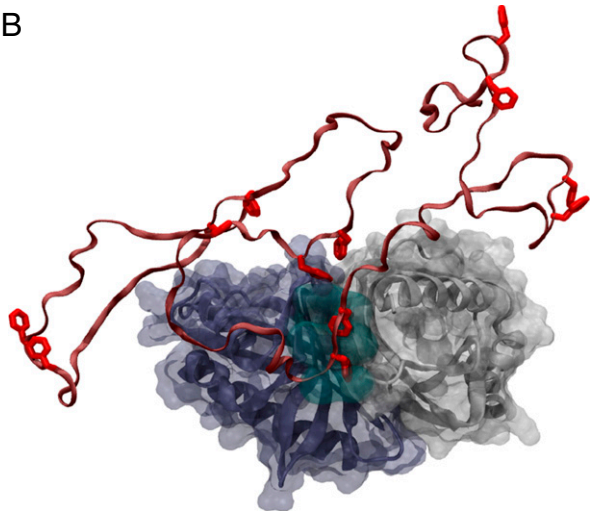

Fig. 1. Simulated system. (*A*) Sequences of FG repeat model constructs. Bold, FSFG motif; underlined, motif bound at crystallographic binding site; blue, positive; red, negative; green, polar. (*B*) Starting conformation for bound $FSFG_6$:NTF2 simulations, with the third FSFG motif initially bound at the crystallographic binding site (cyan space-fill), adapted from pdb-id 1GYB (66).

with TFs (29). Such high-speed FG–TF interactions have been recently observed by stopped-flow measurements (30). However, experimental methods are typically unable to provide details of local interaction site dynamics at atomic resolution and at multiple timescales, spanning a range from individual molecular interactions to the entire transport event. Therefore, an atomic resolution characterization of the interactions between TFs and FG repeats remains to be determined. To address this need, we performed molecular dynamics (MD) simulations combined with NMR experiments to provide an integrated view of dynamic TF/FG repeat interactions at atomic scale from nanoseconds to milliseconds.

MD simulations have already been used to study the interaction of FG repeats with transport factors (31–33). Previous studies have focused on identifying the presence of putative FG repeat interaction sites for each of the transport factors Kap95 and NTF2 (31, 33). Both transport factors were predicted to have multiple interaction sites for FG repeats; these results agree with NMR studies (29, 34). More recently, multiple short simulations of FG repeats were performed in the presence of TFs (30). In these simulations, FG repeats bound readily to TFs, but formed a more compact state than expected based on small-angle X-ray scattering (SAXS) data obtained in the same study (35). Recently, a modified water model was introduced in an attempt to better reproduce the biophysical properties of disordered proteins (36) and FG repeats in particular (35). In our study, we set out to characterize the kinetics of the interaction between TFs and FG Nups and the effect of this interaction on the transport through the NPC. We used long-timescale MD simulations on the Anton supercomputer (37) and state-of-the-art water models designed and tested on disordered and globular proteins (36, 38). We cross-calibrated our simulations with atomic-scale dynamic information provided by our NMR experiments.

As a representative TF, we chose the Ran transport factor NTF2 (13, 39) because of its relatively small size, preferential affinity for the FxFG flavor of repeats, and because it is representative of a major class of transport factors (NTF2 itself and the primary mRNA export factor, Mex67/Mtr2). NTF2 has already been studied by computer simulation, crystallography, and NMR spectroscopy, providing us with a firm experimental background for our studies (32, 34, 40). We use model constructs with two or six FG repeats that contain the FSFG flavor of FG motifs (Fig. 1), which we have previously characterized experimentally (29); we denote these constructs $FSFG_2$ and $FSFG_6$. Both constructs are derived from the yeast FG Nup Nsp1, which is believed to contribute a significant mass of the FG repeats in the central channel of the yeast NPC, and for which again we have detailed dynamic atomic-scale data (29). The simulations show remarkable agreement with experimental data, and provide additional kinetic and thermodynamic properties of the transport system at a level of detail currently inaccessible to experimental methods. Taken together, our results suggest an explanation for how rapid exchange of TFs during nucleocytoplasmic transport may be achieved without compromising interaction selectivity.

Results

We simulated $FSFG_2$ and $FSFG_6$, both in the presence of NTF2 and in their free form, using the AMBER99SB-ILDN force field (41) and with either the TIP4P-Ew (42) or the TIP4P-D (36) water models. The TIP4P-Ew water model reproduces a number of experimental measurements for disordered cyclic peptides, vasopressin and oxytocin (43), and amyloid-β proteins (38, 44). The new TIP4P-D model has increased water dispersion interactions and better approximates global conformational properties of intrinsically disordered proteins (IDPs) (36, 45) and FG repeats in particular (35), enabling more accurate simulation of protein dynamics. *SI Appendix*, Table S1 *A* and *B* summarizes the different simulations conducted in this study, in which we vary the system components, water model, and conformational sampling method.

Biopolymer Properties of FSFG Repeats in TIP4P-Ew and TIP4P-D Water Models. As expected from previous studies (7, 46) and in accordance with our recent NMR analysis (29) (BMRB database entry 25183; ref. 47), the $FSFG_2$ and $FSFG_6$ constructs remained intrinsically disordered and devoid of stable secondary structure segments throughout the simulations, regardless of the water model (Fig. 2*A*; *SI Appendix*, Fig. S1; Movies S1 and S2). A few short and transient β-hairpins did form, but generally dissolved within a few hundred nanoseconds, irrespective of the presence or absence of NTF2 (*SI Appendix*, Fig. S1). However, the choice of water model markedly affected other key biopolymer properties of the FG repeats, both in the free form and in the presence of NTF2. The global conformational properties of FG repeats simulated with the TIP4P-D model are in better agreement with previous experimental observations than those from the TIP4P-Ew simulations. Specifically, in the TIP4P-Ew simulations, the FG repeats formed a relatively compact disordered ensemble with (*i*) a Flory exponent $\nu = 0.35$ characterizing the power dependence of the radius of gyration (R_g) on chain length (48) (Fig. 2*B*) (according to Flory's theory of polymers, a value of 0.33–0.40 is typical for polymers in poor solvent such as globular proteins or premolten globules; ref. 49); (*ii*) a bimodal distribution of distances between consecutive FG repeats with a dominant peak at a relatively short distance of 19.3 Å and a narrow SD of 6.6 Å (Fig. 2*C*); (*iii*) a distribution of radii of gyration (R_g) with a low mean and a narrow SD (*SI Appendix*, Fig. S2); (*iv*) formation of metastable conformational states on the timescale of nanoseconds to microseconds (*SI Appendix*, Fig. S3);

Downloaded by guest on February 24, 2022

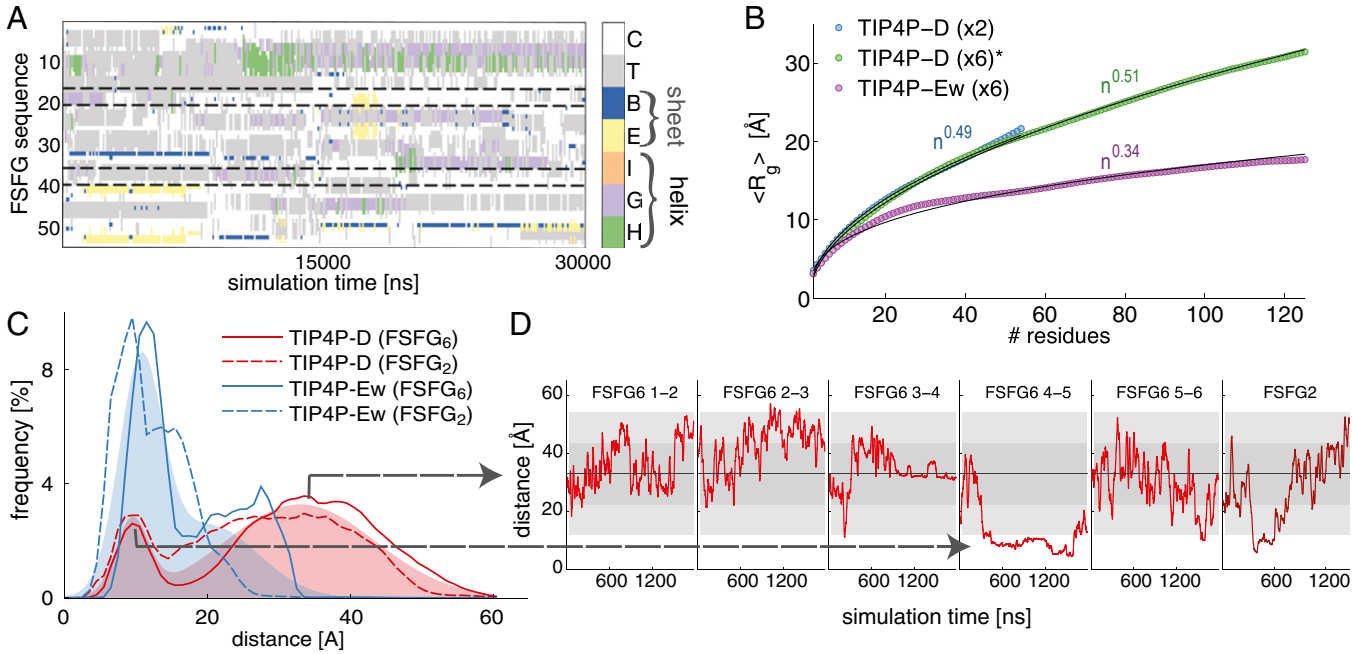

Fig. 2. Biopolymer properties of FSFG repeats. (*A*) The secondary structures assigned to $FSFG_2$ by the program STRIDE (88) throughout the 30-μs-long TIP4P-Ew simulation of $FSFG_2$:NTF2. Helical or sheet secondary structures did not form during the simulations. See *SI Appendix*, Fig. S1 for secondary structure assignment in additional simulations. (*B*) Mean radius of gyration as a function of segment length in TIP4P-D or TIP4P-Ew simulations of $FSFG_6$:NTF2 and $FSFG_2$:NTF2 in the different water models. The Flory exponent was extracted by fitting to power law n^F, where n is the segment length. (*C*) Distribution of distances between adjacent FG motifs in the presence of NTF2 using the TIP4P-D and TIP4P-Ew water models, computed in 1-Å bins. A bimodal Gaussian fit to the average over each water model is shown in space-fill for TIP4P-D (pink) and TIP4P-Ew (blue). (*D*) Change in end-to-end distance between consecutive FG motifs in TIP4P-D simulations, with fast fluctuations around the dominant peak on the nanosecond timescale.

and (*v*) a relatively high probability of intrachain hydrophobic contacts, albeit significantly lower than for a globular protein such as NTF2 (*SI Appendix*, Fig. S4). In contrast, in the TIP4P-D simulations, the FG repeats form an extended disordered ensemble (50, 51) in excellent agreement with the experimental data (50), with (*i*) a Flory exponent $\nu = 0.48$–0.51, the "theta"-solvent regime where attractive and repulsive interactions balance each other, preventing the polymer from either collapsing to a molten globule or swelling (Fig. 2*B*, Movie S1; ref. 49); (*ii*) a distribution of distances that, although bimodal as with TIP4P-Ew, features a dominant peak at a greater distance of 33.0 Å with a broad SD of 10.5 Å (Fig. 2*B*); (*iii*) a distribution of radii of gyration (R_g) with a high mean value and broad SD (*SI Appendix*, Fig. S2); (*iv*) rapid transition between states within nanoseconds and no formation of metastable states (*SI Appendix*, Fig. S3); and (*v*) a low number of intrachain hydrophobic contacts with no hydrophobic core formation (*SI Appendix*, Fig. S4).

The TIP4P-D model seems more appropriate to describe the disordered FG repeats than the TIP4P-Ew model, as intended (35, 36). The reason is that the reported radius of hydration (R_h) measured by dynamic light scattering (29) and the Stokes radii (R_S) determined by size-exclusion chromatography (15) for FxFG flavor Nups strongly argue against $FSFG_6$ adopting a compact disordered ensemble (predicted to have lower R_h or R_S values; refs. 52, 53). In addition, independent SAXS studies of human Nup153 FG repeats with similar sequence properties to $FSFG_6$ also indicate an extended disordered state showing better agreement with TIP4P-D simulations than with TIP4P-Ew simulations (35). Finally, our previously reported NMR relaxation measurements do not suggest significant intrachain contacts for $FSFG_6$ (29). Taken together, these results demonstrate that FG repeats form a classical, completely disordered random coil with no stable intramolecular interactions.

FG Nups Are Fast-Moving Entropic "Springs." That the FG repeats in the TIP4P-D simulations resemble a Flory polymer in theta-solvent (Fig. 2*B*) indicates that they can be modeled as an ideal freely jointed chain (FJC) or its continuous extension, the wormlike chain (WLC) (49, 54). In the latter case, the polymer is treated as a semiflexible rod with a typical persistence length that quantifies its stiffness (55). The computed persistence length in the TIP4P-D simulations indicates a remarkable level of flexibility, ranging from 6.0 to 7.4 Å in the $FSFG_6$:NTF2 and $FSFG_2$:NTF2 simulations, respectively. This stiffness implies that the backbone of the FG repeats is rigid only over the span of two consecutive peptide bonds, in agreement with single-molecule force spectroscopy data for Nup153 (26). According to both the FJC and WLC (with short persistence length) models, the polymer behaves as an entropic "spring" that resists perturbations to its length and radius of gyration similarly to an ideal Hookean (linear elastic) spring. This behavior arises from differences in configurational entropy in macrostates of varying end-to-end distances (49) (*SI Appendix* Methods, Eqs. **S4–S7**; for derivation of the FJC and WLC energy potential for an unconstrained polymer). The entropic spring assumption is in good agreement with the dominant Gaussian peak observed at 33.0 ± 10.5 Å in the distribution of interrepeat distances (Fig. 2*C*, Movie S1). The spring rapidly transitions between these macrostates on the timescale of nanoseconds (Fig. 2*D*); the second, minor peak observed at 10 Å is likely due to weak and transient interactions that temporarily stabilize the chain conformation at this shorter distance (Fig. 2*D*), and thus does not correspond to an entropic spring. Fixing the length of the FG repeats at 10 Å would entail a considerable free energy penalty due to the loss of configurational entropy, thus disfavoring static interactions between two FG motifs at this distance. Although thinking of FG repeats as springs may be an oversimplification, the concept does capture significant elasticity of the FG repeats that results in

Downloaded by guest on February 24, 2022

entropically driven resistance to compression favored by interactions with TFs. This elasticity helps the TF jump from one FG repeat to another, in turn resulting in rapid diffusion through the NPC.

Multiplicity of Interaction Sites on NTF2. TFs, such as Kap95 and NTF2, were previously suggested to use multiple interaction sites for FG motifs based on NMR chemical shift analysis (34) and simulation (33). Most recently, the export factor Crm1 was crystallized with eight simultaneously bound FG motifs from three regions of the FG Nup Nup214 (56). Indeed, in both the TIP4P-D and TIP4P-Ew simulations, the FSFG motifs formed multivalent contacts at many different sites (*SI Appendix*, Fig. S5*A*), including at previously experimentally determined sites (13, 34) and sites suggested from simulations (33). In particular, we observed that a large number of interactions formed at the hydrophobic groove that bridges the two monomers of NTF2 and contains (but is not restricted to) the crystallographic binding site. NMR titration experiments of [U-^{15}N] NTF2 that were performed with increasing concentrations of $FSFG_6$ showed good agreement with the TIP4P-D simulation of $FSFG_6$:NTF2 (*SI Appendix*, Fig. S5*B*), including the clustering of contacts at the hydrophobic groove. These results indicate that TFs, such as NTF2, have a surprisingly large surface area associated with FG motif interaction.

Contributions from FG Motif Residues. The FG motif residues generally contributed strongly to the FSFG:NTF2 interaction, in particular in FG motifs 3, 4, and 5, and to a lesser extent, motif 1 (*SI Appendix*, Fig. S6*A*). Because the six repeats of $FSFG_6$ have nearly identical sequences (Figs. 1*A* and 3*A*) and share similar chemical environments according to our recent NMR studies (29), we were able to reduce the standard errors associated with each individual repeat and significantly amplify the signal-to-noise ratio by averaging over the 19 residues of the FG repeat units (Fig. 3*B*). As expected, the average contribution of the FG motif residues was much larger than for the spacer residues.

Interaction Dynamics. Our recent NMR measurements have demonstrated that the FG repeats of $FSFG_6$ undergo rapid exchange at their interaction sites on Kap95 (29); this rapid exchange was also reported for a different sequence of FG repeats from hNup153 during the interaction with several TFs of different structural architectures, including hNTF2, importin-β, and hTRN1 (30). These recent NMR measurements also showed that FG repeats remain highly disordered while transiently interacting with TFs (29, 30). However, the thermodynamics and kinetics of this rapid exchange are not yet understood. To describe the dynamics of the $FSFG_6$ construct during its interaction with NTF2, we experimentally measured the R_2/R_1 ratio for the *N*–H bonds of each of its (nonproline) residues in the presence of NTF2 (*SI Appendix*, Fig. S6*B*) and averaged again over the 19 residues of the FG repeat (Fig. 3*C*). The FG motif residues, which contribute most strongly to the interaction with NTF2, displayed elevated R_2 values indicative of slower motion of these interacting residues, consistent with previous studies (29, 30). We expect contributions from chemical exchange (R_{ex}) to be limited as previously noted (29). Next, we compared the experiments to simulations by computing theoretical R_2/R_1 ratios from our TIP4P-D simulations of $FSFG_6$ in the presence of NTF2 (Fig. 3*C*; *SI Appendix*, Fig. S6*B*). Indeed, the R_2/R_1 ratio for the FG motif residues that interact with NTF2 (repeats 1, 3, 4, and 5 of $FSFG_6$) were elevated. The corresponding order parameters (S^2) computed from the simulations are shown in *SI Appendix*, Fig. S6*C*; Table S3. These observations are consistent with our prior findings (29) that the exchange rate of FG motifs with their TF interaction sites is fast.

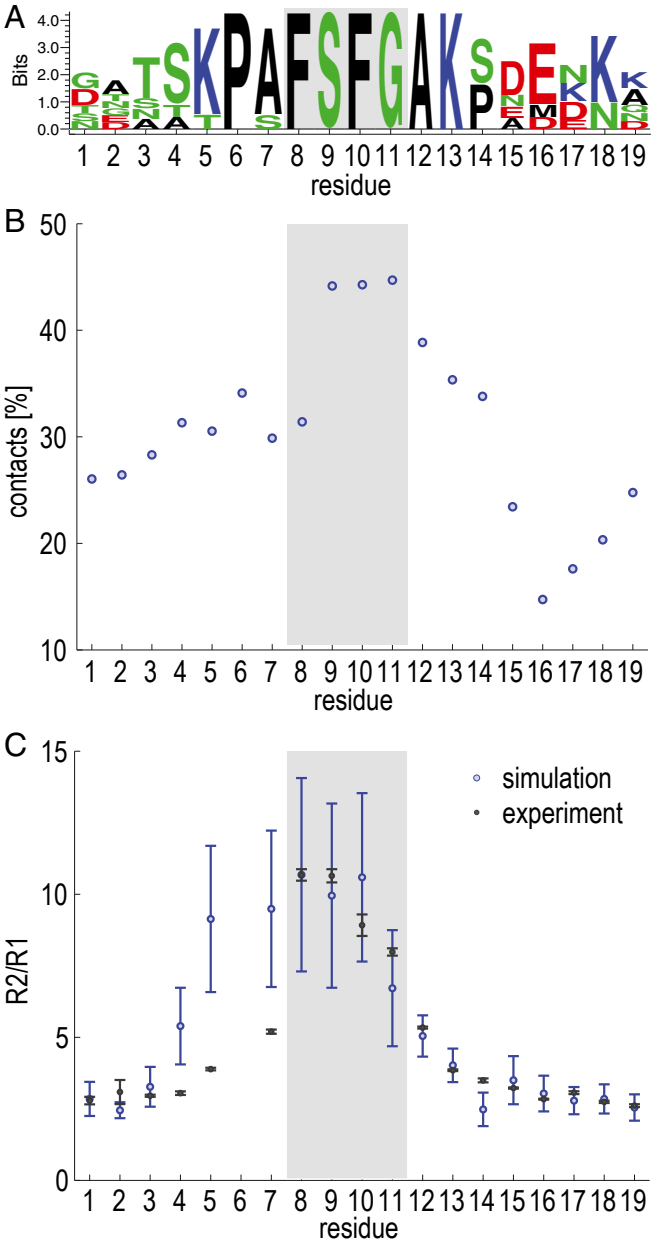

Fig. 3. Binding dynamics to NTF2. (*A*) Sequence profile of the six FG repeats in $FSFG_6$. (*B*) The fraction of simulation time in which different $FSFG_6$ residues are in contact (<5 Å distance between any pair of heavy atoms) with NTF2 during the TIP4P-D simulation, averaged over all residues in corresponding repeat positions. (*C*) R_2/R_1 relaxation values measured experimentally by NMR (black) and in the $FSFG_6$:NTF2 simulations (red). Sequence position 14 represents S alone. See *SI Appendix*, Fig. S6 for nonaveraged data for the entire sequence of FSFG.

Possible Role for Spacer Residues. The simulations also revealed that several spacer residues form transient contacts with NTF2 (Fig. 3; *SI Appendix*, Fig. S6; Movie S2). Spacer residues were previously observed at the interaction interface in the crystal structure of the high-affinity complexes between the TFs Kap95 and CRM-1 (56) and FG Nups Nup1 and Nup214 (pdb-id 2bpt; ref. 57), respectively. However, the predicted R_2/R_1 ratios of the spacer residues that interact with NTF2 (except those immediately adjacent to the FSFG motifs) are not elevated (cf. Fig. 3 *B* and *C*), in agreement with experimental values (Fig. 3*C*). The

Downloaded by guest on February 24, 2022

combination of high contact rate and low R_2/R_1 ratio suggests that these spacer residues contribute only transient and low-specificity contacts, but may assist in briefly anchoring adjacent FG motifs to NTF2. These interactions may lower the free energy barrier to forming and breaking specific FG-motif:NTF2 contacts. The elevated R_2/R_1 ratio in the residues that immediately flank the FG motif may be attributed to their proximity to the bound FG motif, but may also be due to transient hydrophobic contacts of the proline residue that preceded the FG motif (consensus position 7 in Fig. 3*A*).

Sliding Motion in a Lower-Dimensional Space. Our simulations are validated by their reproduction of key experimental observations (Figs. 2 and 3). Thus, we may use our simulations to describe other aspects of the interaction dynamics that are not accessible to experiments. Specifically, we observed that the simulated FG motifs do not interact statically in a single well-defined pose with NTF2, but rather exhibit a significant degree of local motion and remain partially localized to the TF. We termed this local motion "sliding," because the FG motif maintains contact with NTF2 as it slides along the surface, remaining at least partially localized. The sliding motion was observed (in our TIP4P-D water simulations) at the primary, crystallographically observed binding site, where FG motifs tend to slide laterally along the hydrophobic groove at the interface between the two NTF2 subunits (Fig. 4), as well as at alternative sites where an FG-repeat sliding-and-displacement event occurs (see below). After sliding out of the crystallographic binding site, the FG motifs either slide back to the original strongly interacting conformation, or slide out completely and disengage from NTF2 (Fig. 4; Movies S3, S4, and S5). This decrease in apparent dimensionality may result in increasing the rate of a key step in macromolecular transport through the pore; less time is spent exploring possible conformations because the search is constrained to a limited surface.

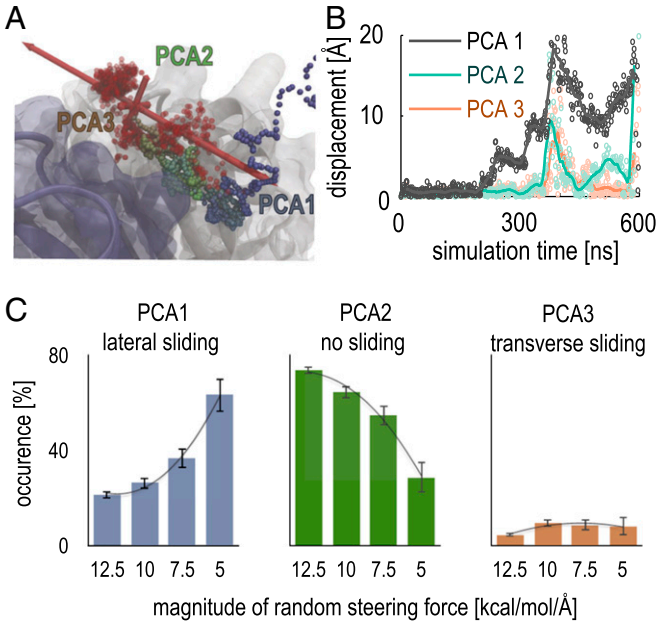

Fig. 4. Sliding of the FG motif residues along the crystallographic binding groove. (*A*) Superposition of the centers of mass of the FG motif residues (FSFG) at the crystallographic binding site from 10 independent TAMD simulations with the TIP4P-Ew water model (red spheres), and their principal components scaled by their eigenvalues (red arrows), showing a favorable lateral sliding mode of motion (PCA1). The NTF2 subunits are shown in blue and gray ribbon/surface representation. The trace of the center of mass of the same FG motif during the first 400 ns of the unbiased bound $FSFG_6$:NTF2 simulation with the TIP4P-D water model is shown in a color gradient of spheres from its initial conformation ($t = 0$ ns; orange) to the final unbinding event ($t = 400$ ns; blue), as it slides along PCA1 ($t = 200$ ns; green) (Movies S3 and S4). (*B*) The principal component values during the unbinding in the unbiased $FSFG_6$:NTF2 simulation shown in *A* and in Movies S3 and S4. (*C*) Occurrence of motions over 5 Å along the different principal components for RAMD simulations with decreasing random force magnitude (*x* axis). A random force of magnitude 0 kcal mol^{-1} $Å^{-2}$ is equivalent to an unbiased simulation. Trend lines from a polynomial fit are plotted in gray.

Robustness of Sliding to Water Model. We attempted to enhance the sampling in our TIP4P-Ew simulations using temperature-accelerated molecular dynamics (TAMD) (58, 59) to determine whether the sliding motion is sensitive to the choice of water model. We accelerated the transition rate between system states by imposing a TAMD restraint on a pair of spacer residues, without directly biasing the motion of the FG motif (*Methods*). In 10 independent TIP4P-Ew TAMD simulations, the FG motifs exhibited significantly increased sliding motion similar to that of the unbiased TIP4P-D simulations. We applied principal component analysis (PCA) to the coordinates of the center of mass of the FG motif at the crystallographic binding site (residues 50–53) in the TIP4P-Ew TAMD simulations (Fig. 4 *A* and *B*; *SI Appendix*, Fig. S6). The first principal component of the centers of mass accounts for 71.5% of the variance (*SI Appendix*, Table S2). This principal component corresponds to the exact one-dimensional motion along the groove that we observed in the TIP4P-D unbiased simulations. Hence, the tendency of FG motifs to slide on NTF2 does not depend on the choice of water models used here.

Propensity for Sliding. To assess the predominance of sliding over other modes of motion, we complemented our Anton simulations with 5,400 independent and relatively short (150–1,500 ps) randomly accelerated molecular dynamics (RAMD) simulations (60) of a single FG motif at the NTF2 crystallographic binding site, for a total of 3,820 ns of simulations. In contrast to most enhanced sampling methods, RAMD has often been used to find favorable modes of motion of a ligand or structural element and avoid a priori assumptions about the direction of motion (61, 62). Using RAMD, we iteratively applied a randomly oriented steering force of fixed magnitude to the FG motifs, setting the magnitude of the steering force between 5.0 and 12.5 kcal mol^{-1} $Å^{-1}$ in different simulations. When the external force was strong (12.5 kcal mol^{-1} $Å^{-1}$), the propensity for sliding along PCA1 was only 22%, but increased to 64% as the external force was decreased to 5.0 kcal mol^{-1} $Å^{-1}$ (Fig. 4*C*, Movie S6). By extrapolation, the propensity for sliding is likely to be even higher as the random force reaches zero and the simulations become unbiased. We conclude that an FG motif favors sliding along the hydrophobic groove at the interface between the two NTF2 monomers. Next, we address the question of whether or not this sliding results in faster exchange of bound FG motifs.

Slide-and-Exchange by FG Repeats. As the FG motifs slide along PCA1 (*SI Appendix*, Fig. S8, Movie S5), the original atomic contacts are broken and new contacts are formed. This transition from a strongly interacting state to a weakly interacting state is stabilized by weak nonnative contacts, and leaves the interaction pocket partially accessible. As one FG motif slides to this weakly interacting state, competing FG motifs may slide into the interaction pocket and displace the previously strongly interacting motif. Indeed, in our longest simulation (a 32-μs simulation of $FSFG_2$ and NTF2), one of the FG motifs was observed to slide along the NTF2 surface, displacing an FG repeat that was interacting at a noncrystallographic site (Fig. 5*A*, Movie S7). Furthermore, in one of our unbiased simulations of $FSFG_2$ and NTF2 in TIP4P-D water, we observed two FSFG repeats interacting simultaneously at the crystallographic binding site (Fig. 5*B*, Movie S8).

PNAS PLUS
BIOPHYSICS AND COMPUTATIONAL BIOLOGY
APPLIED PHYSICAL SCIENCES
Downloaded by guest on February 24, 2022

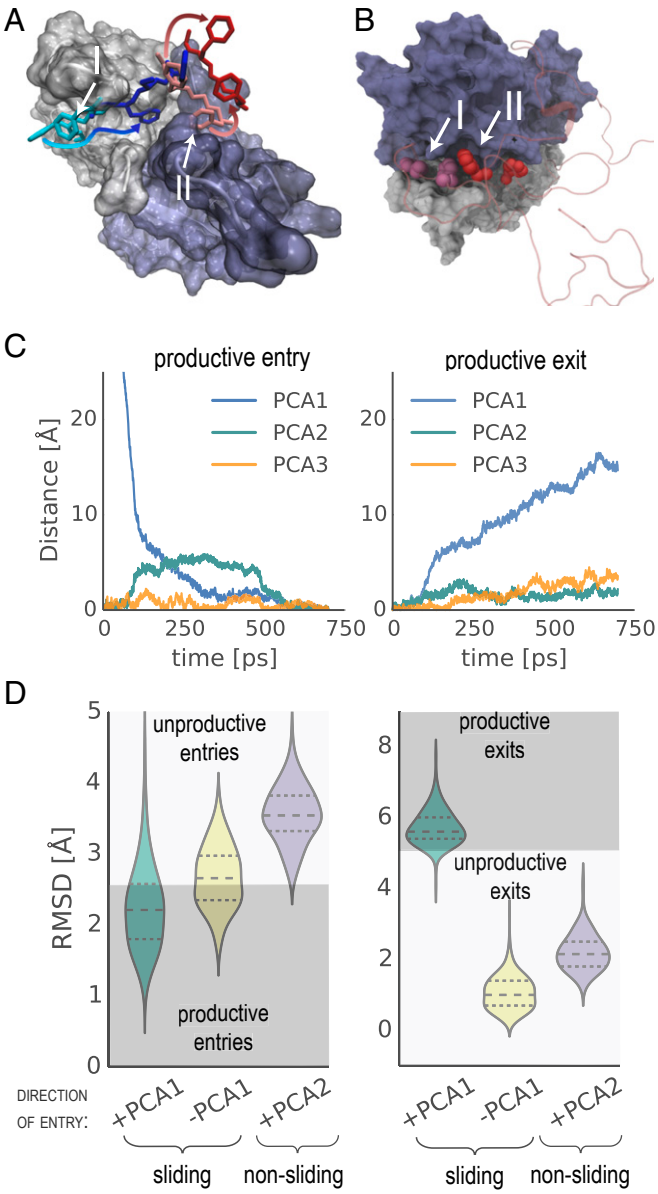

Fig. 5. A sliding-and-exchange mechanism. (*A*) A strongly interacting motif slides out (motif II; pink to red) to a weakly interacting state as a competing motif (motif I; cyan to blue) slides in Movie S7 in the unbiased TIP4P-Ew simulation of $FSFG_2$:NTF2. (*B*) Two individual FG motifs (magenta and red space-fill, indicated as I and II) accommodated simultaneously at the crystallographic binding site on the NTF2 dimer along the horizontal binding groove in the unbiased TIP4P-D simulation of $FSFG_6$:NTF2. (*C*) A representative exchange trajectory (similar to other productive exchange trajectories which comprise 97% of all trajectories), showing the distance from the interaction site of either the displacing (*Left*) or displaced FG motif (*Right*), projected over each of the three principal components (as in Fig. 4*A*; *SI Appendix*, Table S2). See also Movie S9. (*D*) Distribution of productive vs. nonproductive exchange events in the targeted MD simulations (63), in which the displacing FG motif was targeted toward the interaction site from either the +PCA1, −PCA1, or +PCA2 directions. A productive exchange event requires productive entry (*Left*) and exit (*Right*), assessed here according to the final root-mean-square-deviation (RMSD) from the interaction site of either the displacing or displaced FG motifs, respectively.

Because the experimental data indicate that the exchange of FG motifs occurs on the timescale of several microseconds (29), the exchange is a relatively rare event even on the timescale of the unbiased Anton simulation. To increase our confidence that such rare simulated events nevertheless reflect the nature of the actual process, we complemented the Anton simulations and the RAMD simulations with an additional 1,500 independent targeted MD simulations (63), each simulated for 700 ps (a total of 1,950 ns). In each of these simulations, an unbound FG motif (motif 1) was targeted toward an interaction site on NTF2, which was in turn initially occupied by a second FG motif (motif 2). Motif 1 was targeted toward NTF2 from either the +PCA1 sliding direction, from the opposing −PCA1 sliding direction, or from the +PCA2 nonsliding direction (PCAs as indicated in Fig. 4*A*; *SI Appendix*, Table S2).

As expected, when motif 1 was targeted toward the interaction site starting from the +PCA1 direction, it readily entered the interaction site in 69% of the simulation trajectories (Fig. 5 *C* and *D*, *Left*) and promoted the complete ejection of motif 2 out of the interaction site in 98.5% of the simulation trajectories (Fig. 5 *C* and *D*, *Right*; Movie S9). In contrast, the exchange was mostly nonproductive when motif 1 entered the binding site from the +PCA2 nonsliding direction. In addition, the sliding was asymmetric with respect to the sliding direction, and was disfavored when motif 1 approached the interaction site from the −PCA1 sliding direction. Lastly, in 97% of the productive exchange events, motif 2 was ejected from the interaction site in the PCA1 sliding direction, as motif 1 approached the interaction site, as in the representative trajectory plotted in Fig. 5*B* and shown in Movie S9. Thus, reversible sliding in and out of the binding site along PCA1 may indeed provide a direct and energetically favorable mechanism for fast exchange of FG Nups with TFs.

Discussion

The interaction between FG Nups and TFs lies at the heart of nucleocytoplasmic transport. Several mesoscale models have been proposed to explain the transport mechanism (21), though none describes FG–TF interactions at the atomic level of detail. Our previous experimental studies (29), as well as independent studies from other groups (30), indicate that TFs associate and dissociate from FG motifs at an exceptionally fast rate. This fast exchange may reconcile the apparent discrepancy between transport that is rapid on the one hand, and selective on the other (Fig. 6*A*). However, the underlying mechanism of this exchange is unknown. Based on our unbiased long-timescale simulations, supported by enhanced-sampling simulations and NMR experimental measurements, we have identified a strong tendency of FG motifs to transition rapidly between the strongly interacting and weakly interacting states through sliding in and out of interaction pockets on the surface of a TF (Fig. 4). These rapid transitions provide an efficient mechanism for fast exchange of FG motifs through competitive displacement (Fig. 5), compared with a much slower exchange expected for a two-state interaction mechanism that requires full disengagement and reengagement. In summary, we suggest the following key features result in rapid FG repeat exchange on TFs, thus facilitating the rapid translocation of TFs during nucleocytoplasmic transport without compromising transport specificity (Fig. 6*B*): (*i*) rapid kinetics of individual FG motif–TF interactions due to sliding (Figs. 4 and 5; *SI Appendix*, Figs. S7 and S8); (*ii*) anchor points for fast exchange on the surface of TFs due to multiplicity of TF interaction sites (*SI Appendix*, Fig. S5) and transient interactions by spacer residues (Fig. 3; *SI Appendix*, Fig. S6); and (*iii*) intrinsic elasticity of the FG repeats favoring dynamic interactions and resisting entropic restriction due to static interactions (Fig. 2; *SI Appendix*, Figs. S1–S4).

Biophysical Properties of TFs and FG Motifs That Enable Sliding. It has previously been suggested that proteins may slide on DNA (64) or during interactions between globular proteins (65). Here, we extend this concept to sliding of disordered interaction motifs on globular proteins. The dynamic nature of the interacting state of

Downloaded by guest on February 24, 2022

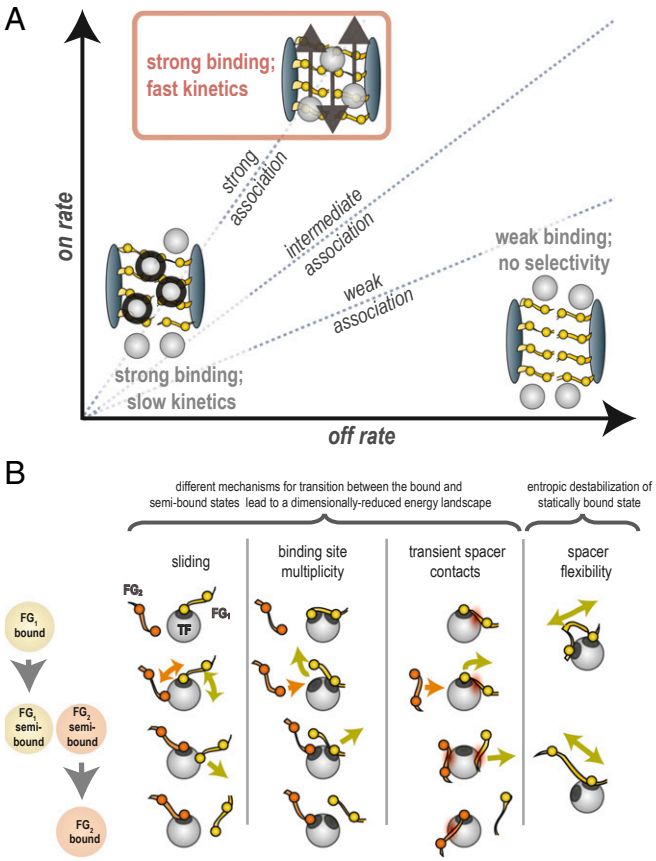

Fig. 6. Balancing transport rate and selectivity. (*A*) Efficient nucleocytoplasmic transport requires strong binding affinity and a high off rate to guarantee fast exchange of TFs interacting with FG repeats. (*B*) Mechanisms for fast partial unbinding and rebinding in a dimensionally reduced energy landscape, compared with complete unbinding and rebinding.

the NTF2 and FG repeats may explain why crystallization of the NTF2:FSFG complex required the N77Y mutant NTF2, that binds FG motifs significantly more tightly than wild-type NTF2. In the strongly interacting mutant, transport is slower compared with wild-type NTF2, attesting to the likely functional role of a dynamic binding mechanism in facilitating efficient nucleocytoplasmic transport (66) as well as a fine-tuned affinity for FG/TF interactions. Hence, although the experimental evidence overwhelmingly suggests that NTF2 is specifically tailored to interact with FG repeats (67) and to transport 120 times faster than similarly sized molecules (22), both NTF2 and the FG repeats seem to possess certain geometric and chemical features that lower the energy barrier to sliding. From a biochemical point of view, these features may include the following: (*i*) A relatively large and elongated interacting groove on NTF2, which could restrict the sliding direction and enable competing FG motifs to approach the interaction site simultaneously (Fig. 5*A*); (*ii*) the presence of multiple hydrophobic residues at close proximity to the interaction site that could streamline the motion of the FG motifs along the interaction site and disfavor its complete dissociation from the TFs, as also evidenced by the patch of chemical shift perturbations on NTF2 upon binding to FG repeats (Fig. S5), and by the fact that increased surface hydrophobicity promotes fast transport even in non-TF proteins (68); (*iii*) the intrinsic flexibility of the FG spacer regions that further disfavors static binding due to the entropic penalty of restraining flexible molecules; and (*iv*) the entropic benefit of interacting dynamically rather than statically. It remains to be seen whether such a specific-yet-dynamic mechanism of interaction is prevalent in other classes of disordered proteins and globular proteins, in particular in transient-yet-specific interactions, which are underrepresented in databases of protein interactions due to their lower signal in experimental assays (69).

FG Motifs as Dynamic Probes. The reduced dynamics of the FG motif residues, which were observed both experimentally (29) and here *in silico*, originated in the simulations not only from the strong interactions between the FG motifs at the crystallographic binding site, but also from transient and apparently nonspecific contacts between various patches on the surface of NTF2 in the weakly interacting state (Figs. 3 and 4). Slower dynamics of FG motif residues were observed not only in the presence of TFs, but also in NMR measurements of FSFG in *Escherichia coli* cells and in lysates, which do not contain TFs, yet those relaxation measurements produced a similar signal to that observed in the presence of TFs (29). We suggest that the relatively hydrophobic nature of phenylalanine residues, their ability to form π-interactions with charged residues, the relatively long distance of their sidechains from the backbone, and the structural flexibility of the adjacent glycine residues turns the phenylalanine-glycine motifs into perfect probes for rapid binding moieties. These motifs readily and nonspecifically interact with protein surfaces, but the surface of specific TFs is tuned to funnel them toward stronger interactions at multiple sites and to enable surface sliding between strongly interacting and weakly interacting states. This high degree of interacting state dynamics promotes fast exchange and selective transport of TFs.

Direct Function for Intrinsic Disorder. Disordered proteins are well-established mediators of protein–protein interactions through incorporation of short linear binding motifs and/or through folding upon binding (50). Nevertheless, the direct role of protein disorder itself in function is often overlooked. FG Nups provide an intriguing model system where the intrinsic polymer properties of the disordered FG repeat domains contribute directly to rapid diffusion of TFs through the NPC. According to our simulations and experimental measurements, the FG repeats most closely resemble a classic random coil with spacer regions acting as soft entropic springs between consecutive FG motifs (Fig. 2, Movie S1). The resulting structural plasticity enables the relatively free movement of interacting FG motifs in the context of full FG repeat domains, and disfavors static interactions due to the large entropic penalty for constraining a flexible chain. The spacer regions may form nonspecific and transient interactions with NTF2, both providing anchors for rapid recontacting of loose FG motifs, and resulting in a weak multivalency effect. As already suggested (70), electrostatic interactions between the disordered regions and TFs may also play a role similar to the well-characterized effect of electrostatic steering on the kinetics of protein–protein interactions (71). We also observed electrostatic steering due to long-range interaction between the multiple lysine residues in the FG motifs and the acidic patch on NTF2 (residues 91–93), which we shall further investigate in future work.

Toward a Comprehensive Model of Transport. Our simulations describe important microscopic aspects of the FG–TF interaction at an atomic-level resolution, aspects that are not explicitly considered by any of the previously proposed mesoscale models of nucleocytoplasmic transport (1, 3, 15, 23–28, 72). Nonetheless, it is informative to assess our results in the context of those models. We do not observe *in silico* any significant inter-FG motif interactions, which is a prominent tenet of the hydrogel model (24). Instead, the highly dynamic, extended random coil behavior of the FG Nups, the lack of intrachain interactions, and the entropic resistance to spatial confinement are consistent with some key aspects of the virtual gate/polymer brush models

Downloaded by guest on February 24, 2022

(23, 27). The different flavors of FG repeats (15) have been proposed to play different roles in transport and interaction with specific ligands (15, 16, 73–75). Correspondingly, NTF2 is a representative of the NTF-like family of TFs, and TFs of the karyopherin-β family adopt an entirely different structural architecture (76). Nevertheless, both families of TFs have evolved, perhaps convergently, to interact with FG motifs through hydrophobic pockets defining multiple binding sites on the surface of a TF (77). They also show similar interaction dynamics as reported here for NTF2 (29, 35), suggesting that they are transported through a similar mechanism to that of NTF2. Therefore, it seems likely that their mechanisms are also similar, although it remains to be seen how changes in the composition of FG Nups affect their biopolymer properties and how these differences are translated to fine-tune the transport system and its interactions with different types of TFs. The effects of confining FG repeats within a constricted channel, and allosteric modulation due to interactions with proteins such as Ran (78, 79) also need to be assessed (9).

In conclusion, we propose that sliding of FG repeats contributes to fast exchange of TFs over a wide range of biophysical states of FG repeats within the NPC. Our findings suggest a mode of interaction between disordered proteins and other macromolecules that is reminiscent of the sliding of transcription factors on DNA (64) or of interactions between globular proteins (65). This mode is fundamentally different from the classic, two-state binding reaction that is often used to describe protein–protein interactions. The ability to interact transiently yet selectively appears to be an evolved property that facilitates dynamic cellular processes, such as the transport of macromolecules through the NPC.

Materials and Methods

The simulations were conducted using a complex of the NTF2 dimer (PDB 1GYB) (66), fully solvated, with the disordered $FSFG_6$ construct in conformations generated by a combination of FlexPepDock (80) and implicit short solvent simulation in AMBER. Simulations of other constructs were performed by modification of this starting system. Systems were equilibrated using standard equilibration protocols (41, 81, 82) in AMBER (83, 84). Long timescale simulations were conducted on the Anton system with a 2-fs time step (85). Temperature accelerated molecular dynamics simulations were also conducted on Anton. Random acceleration MD simulations were set up and equilibrated in AMBER, followed by further equilibration and production runs in NAMD (86). Targeted MD of the FG motif exchange used NAMD with PLUMED 2.2 (87). NMR measurements and analysis of shifts used standard methods (29). Simulation of NMR relaxation used correlation and spectral density analysis of the 1,750-ns TIP4P-D simulation of $FSFG_6$:NTF2 and prediction with ultrafast, fast, and slow components (81). Details of these calculations, of calculation of the Flory exponent, and of the entropic spring model are in *SI Appendix*. A repository of simulations and scripts from methods is available at https://github.com/integrativemodeling/npc_slide_and_exchange.

ACKNOWLEDGMENTS. Simulations used the Anton special-purpose supercomputer provided by the National Resource for Biomedical Supercomputing (NRBSC), the Pittsburgh Supercomputing Center (PSC), and the Biomedical Technology Research Center for Multiscale Modeling of Biological Systems (MMBioS) through Grant P41GM103712-S1 from the National Institutes of Health. D. E. Shaw Research generously made the Anton machine at NRBSC/PSC available. Additional simulations used XSEDE resources supported by National Science Foundation Grant ACI-1053575. J.M.K. was supported by NIH Grant T32 GM007288-39. We were also funded by Grants R01 GM112108, P41 GM109824, U01 GM098256 (to M.P.R. and A.S.), and R01 GM117212 and S10 OD016305 (to D.C.).

1. Rout MP, et al. (2000) The yeast nuclear pore complex: Composition, architecture, and transport mechanism. *J Cell Biol* 148(4):635–651.
2. Wente SR, Rout MP (2010) The nuclear pore complex and nuclear transport. *Cold Spring Harb Perspect Biol* 2(a000562):1–19.
3. Ribbeck K, Görlich D (2002) The permeability barrier of nuclear pore complexes appears to operate via hydrophobic exclusion. *EMBO J* 21(11):2664–2671.
4. Lim RY, Ullman KS, Fahrenkrog B (2008) Biology and biophysics of the nuclear pore complex and its components. *Int Rev Cell Mol Biol* 267:299–342.
5. Simon DN, Rout MP (2014) Cancer and the nuclear pore complex. *Adv Exp Med Biol* 773:285–307.
6. Jamali T, Jamali Y, Mehrbod M, Mofrad MRK (2011) Nuclear pore complex biochemistry and biophysics of nucleoplasmic transport in health and disease. *International Review of Cell and Molecular Biology* 287:233–286.
7. Denning DP, Patel SS, Uversky V, Fink AL, Rexach M (2003) Disorder in the nuclear pore complex: The FG repeat regions of nucleoporins are natively unfolded. *Proc Natl Acad Sci USA* 100(5):2450–2455.
8. Lim RY, Fahrenkrog B (2006) The nuclear pore complex up close. *Curr Opin Cell Biol* 18(3):342–347.
9. Jovanovic-Talisman T, et al. (2009) Artificial nanopores that mimic the transport selectivity of the nuclear pore complex. *Nature* 457(7232):1023–1027.
10. Peters R (2009) Functionalization of a nanopore: The nuclear pore complex paradigm. *Biochim Biophys Acta* 1793(10):1533–1539.
11. Lusk CP, Blobel G, King MC (2007) Highway to the inner nuclear membrane: Rules for the road. *Nat Rev Mol Cell Biol* 8(5):414–420.
12. Gwizdek C, et al. (2003) Exportin-5 mediates nuclear export of minihelix-containing RNAs. *J Biol Chem* 278(8):5505–5508.
13. Bayliss R, et al. (1999) Interaction between NTF2 and xFxFG-containing nucleoporins is required to mediate nuclear import of RanGDP. *J Mol Biol* 293(3):579–593.
14. Allen NP, Huang L, Burlingame A, Rexach M (2001) Proteomic analysis of nucleoporin interacting proteins. *J Biol Chem* 276(31):29268–29274.
15. Yamada J, et al. (2010) A bimodal distribution of two distinct categories of intrinsically disordered structures with separate functions in FG nucleoporins. *Mol Cell Proteomics* 9(10):2205–2224.
16. Patel SS, Rexach MF (2008) Discovering novel interactions at the nuclear pore complex using bead halo: A rapid method for detecting molecular interactions of high and low affinity at equilibrium. *Mol Cell Proteomics* 7(1):121–131.
17. Denning DP, Rexach MF (2007) Rapid evolution exposes the boundaries of domain structure and function in natively unfolded FG nucleoporins. *Mol Cell Proteomics* 6(2):272–282.
18. Campen A, et al. (2008) TOP-IDP-scale: A new amino acid scale measuring propensity for intrinsic disorder. *Protein Pept Lett* 15(9):956–963.
19. Tetenbaum-Novatt J, Rout MP (2010) The mechanism of nucleocytoplasmic transport through the nuclear pore complex. *Cold Spring Harb Symp Quant Biol* 75:567–584.
20. Tran EJ, King MC, Corbett AH (2014) Macromolecular transport between the nucleus and the cytoplasm: Advances in mechanism and emerging links to disease. *Biochim Biophys Acta* 1843(11):2784–2795.
21. Grünwald D, Singer RH, Rout M (2011) Nuclear export dynamics of RNA-protein complexes. *Nature* 475(7356):333–341.
22. Ribbeck K, Görlich D (2001) Kinetic analysis of translocation through nuclear pore complexes. *EMBO J* 20(6):1320–1330.
23. Rout MP, Aitchison JD, Magnasco MO, Chait BT (2003) Virtual gating and nuclear transport: The hole picture. *Trends Cell Biol* 13(12):622–628.
24. Frey S, Richter RP, Görlich D (2006) FG-rich repeats of nuclear pore proteins form a three-dimensional meshwork with hydrogel-like properties. *Science* 314(5800):815–817.
25. Peters R (2005) Translocation through the nuclear pore complex: Selectivity and speed by reduction-of-dimensionality. *Traffic* 6(5):421–427.
26. Lim RY, et al. (2006) Flexible phenylalanine-glycine nucleoporins as entropic barriers to nucleocytoplasmic transport. *Proc Natl Acad Sci USA* 103(25):9512–9517.
27. Lim RY, et al. (2007) Nanomechanical basis of selective gating by the nuclear pore complex. *Science* 318(5850):640–643.
28. Frey S, Görlich D (2007) A saturated FG-repeat hydrogel can reproduce the permeability properties of nuclear pore complexes. *Cell* 130(3):512–523.
29. Hough LE, et al. (2015) The molecular mechanism of nuclear transport revealed by atomic-scale measurements. *eLife* 4(10027):1–23.
30. Milles S, et al. (2015) Plasticity of an ultrafast interaction between nucleoporins and nuclear transport receptors. *Cell* 163(3):734–745.
31. Isgro TA, Schulten K (2005) Binding dynamics of isolated nucleoporin repeat regions to importin-beta. *Structure* 13(12):1869–1879.
32. Isgro TA, Schulten K (2007) Cse1p-binding dynamics reveal a binding pattern for FG-repeat nucleoporins on transport receptors. *Structure* 15(8):977–991.
33. Isgro TA, Schulten K (2007) Association of nuclear pore FG-repeat domains to NTF2 import and export complexes. *J Mol Biol* 366(1):330–345.
34. Morrison J, Yang JC, Stewart M, Neuhaus D (2003) Solution NMR study of the interaction between NTF2 and nucleoporin FxFG repeats. *J Mol Biol* 333(3):587–603.
35. Mercadante D, et al. (2015) Kirkwood-Buff approach rescues overcollapse of a disordered protein in canonical protein force fields. *J Phys Chem B* 119(25):7975–7984.
36. Piana S, Donchev AG, Robustelli P, Shaw DE (2015) Water dispersion interactions strongly influence simulated structural properties of disordered protein states. *J Phys Chem B* 119(16):5113–5123.
37. Klepeis JL, Lindorff-Larsen K, Dror RO, Shaw DE (2009) Long-timescale molecular dynamics simulations of protein structure and function. *Curr Opin Struct Biol* 19(2):120–127.
38. Ball KA, et al. (2011) Homogeneous and heterogeneous tertiary structure ensembles of amyloid-β peptides. *Biochemistry* 50(35):7612–7628.
39. Ribbeck K, Lipowsky G, Kent HM, Stewart M, Görlich D (1998) NTF2 mediates nuclear import of Ran. *EMBO J* 17(22):6587–6598.

Downloaded by guest on February 24, 2022

40. Bayliss R, Littlewood T, Strawn LA, Wente SR, Stewart M (2002) GLFG and FxFG nucleoporins bind to overlapping sites on importin-beta. *J Biol Chem* 277(52): 50597–50606.
41. Lindorff-Larsen K, et al. (2010) Improved side-chain torsion potentials for the Amber ff99SB protein force field. *Proteins* 78(8):1950–1958.
42. Horn HW, et al. (2004) Development of an improved four-site water model for biomolecular simulations: TIP4P-Ew. *J Chem Phys* 120(20):9665–9678.
43. Yedvabny E, Nerenberg PS, So C, Head-Gordon T (2015) Disordered structural ensembles of vasopressin and oxytocin and their mutants. *J Phys Chem B* 119(3): 896–905.
44. Ball KA, Phillips AH, Wemmer DE, Head-Gordon T (2013) Differences in β-strand populations of monomeric Aβ40 and Aβ42. *Biophys J* 104(12):2714–2724.
45. Henriques J, Cragnell C, Skepö M (2015) Molecular dynamics simulations of intrinsically disordered proteins: Force field evaluation and comparison with experiment. *J Chem Theory Comput* 11(7):3420–3431.
46. Lim RY, Köser J, Huang NP, Schwarz-Herion K, Aebi U (2007) Nanomechanical interactions of phenylalanine-glycine nucleoporins studied by single molecule force-volume spectroscopy. *J Struct Biol* 159(2):277–289.
47. Ulrich EL, et al. (2008) BioMagResBank. *Nucleic Acids Res* 36(Database issue): D402–D408.
48. Kaiser A, Babel S, ten Hagen B, von Ferber C, Löwen H (2015) How does a flexible chain of active particles swell? *J Chem Phys* 142(12):124905.
49. Van der Maarel JR (2008) *Introduction to Biopolymer Physics* (World Scientific Publishing Co Pte Lts, Singapore).
50. van der Lee R, et al. (2014) Classification of intrinsically disordered regions and proteins. *Chem Rev* 114(13):6589–6631.
51. Dunker AK, Silman I, Uversky VN, Sussman JL (2008) Function and structure of inherently disordered proteins. *Curr Opin Struct Biol* 18(6):756–764.
52. Marsh JA, Forman-Kay JD (2010) Sequence determinants of compaction in intrinsically disordered proteins. *Biophys J* 98(10):2383–2390.
53. Tcherkasskaya O, Davidson EA, Uversky VN (2003) Biophysical constraints for protein structure prediction. *J Proteome Res* 2(1):37–42.
54. Isralewitz B, Gao M, Schulten K (2001) Steered molecular dynamics and mechanical functions of proteins. *Curr Opin Struct Biol* 11(2):224–230.
55. Receveur-Brechot V, Durand D (2012) How random are intrinsically disordered proteins? A small angle scattering perspective. *Curr Protein Pept Sci* 13(1):55–75.
56. Port SA, et al. (2015) Structural and functional characterization of CRM1-Nup214 interactions reveals multiple FG-binding sites involved in nuclear export. *Cell Reports* 13(4):690–702.
57. Liu SM, Stewart M (2005) Structural basis for the high-affinity binding of nucleoporin Nup1p to the Saccharomyces cerevisiae importin-beta homologue, Kap95p. *J Mol Biol* 349(3):515–525.
58. Voter AF (1997) Hyperdynamics: Accelerated molecular dynamics of infrequent events. *Phys Rev Lett* 78(20):3908–3911.
59. Abrams CF, Vanden-Eijnden E (2010) Large-scale conformational sampling of proteins using temperature-accelerated molecular dynamics. *Proc Natl Acad Sci USA* 107(11): 4961–4966.
60. Lüdemann SK, Lounnas V, Wade RC (2000) How do substrates enter and products exit the buried active site of cytochrome P450cam? 1. Random expulsion molecular dynamics investigation of ligand access channels and mechanisms. *J Mol Biol* 303(5): 797–811.
61. Winn PJ, Lüdemann SK, Gauges R, Lounnas V, Wade RC (2002) Comparison of the dynamics of substrate access channels in three cytochrome P450s reveals different opening mechanisms and a novel functional role for a buried arginine. *Proc Natl Acad Sci USA* 99(8):5361–5366.
62. Pavlova M, et al. (2009) Redesigning dehalogenase access tunnels as a strategy for degrading an anthropogenic substrate. *Nat Chem Biol* 5(10):727–733.
63. Schlitter J, Engels M, Krüger P (1994) Targeted molecular dynamics: A new approach for searching pathways of conformational transitions. *J Mol Graph* 12(2):84–89.
64. Hammar P, et al. (2012) The lac repressor displays facilitated diffusion in living cells. *Science* 336(6088):1595–1598.
65. Kozakov D, et al. (2014) Encounter complexes and dimensionality reduction in protein-protein association. *eLife* 3(e01380):1–21.
66. Bayliss R, et al. (2002) Structural basis for the interaction between NTF2 and nucleoporin FxFG repeats. *EMBO J* 21(12):2843–2853.
67. Strawn LA, Shen T, Shulga N, Goldfarb DS, Wente SR (2004) Minimal nuclear pore complexes define FG repeat domains essential for transport. *Nat Cell Biol* 6(3):197–206.
68. Naim B, Zbaida D, Dagan S, Kapon R, Reich Z (2009) Cargo surface hydrophobicity is sufficient to overcome the nuclear pore complex selectivity barrier. *EMBO J* 28(18): 2697–2705.
69. Hein MY, et al. (2015) A human interactome in three quantitative dimensions organized by stoichiometries and abundances. *Cell* 163(3):712–723.
70. Tagliazucchi M, Peleg O, Kröger M, Rabin Y, Szleifer I (2013) Effect of charge, hydrophobicity, and sequence of nucleoporins on the translocation of model particles through the nuclear pore complex. *Proc Natl Acad Sci USA* 110(9):3363–3368.
71. Schreiber G, Fersht AR (1996) Rapid, electrostatically assisted association of proteins. *Nat Struct Biol* 3(5):427–431.
72. Labokha AA, et al. (2013) Systematic analysis of barrier-forming FG hydrogels from Xenopus nuclear pore complexes. *EMBO J* 32(2):204–218.
73. Terry LJ, Shows EB, Wente SR (2007) Crossing the nuclear envelope: Hierarchical regulation of nucleocytoplasmic transport. *Science* 318(5855):1412–1416.
74. Wozniak RW, Blobel G, Rout MP (1994) POM152 is an integral protein of the pore membrane domain of the yeast nuclear envelope. *J Cell Biol* 125(1):31–42.
75. Popken P, Ghavami A, Onck PR, Poolman B, Veenhoff LM (2015) Size-dependent leak of soluble and membrane proteins through the yeast nuclear pore complex. *Mol Biol Cell* 26(7):1386–1394.
76. Cook A, Bono F, Jinek M, Conti E (2007) Structural biology of nucleocytoplasmic transport. *Annu Rev Biochem* 76:647–671.
77. Stewart M (2007) Molecular mechanism of the nuclear protein import cycle. *Nat Rev Mol Cell Biol* 8(3):195–208.
78. Lee SJ, Matsuura Y, Liu SM, Stewart M (2005) Structural basis for nuclear import complex dissociation by RanGTP. *Nature* 435(7042):693–696.
79. Lowe AR, et al. (2015) Importin-β modulates the permeability of the nuclear pore complex in a Ran-dependent manner. *eLife* 4(04052):1–24.
80. Raveh B, London N, Zimmerman L, Schueler-Furman O (2011) Rosetta FlexPepDock ab-initio: Simultaneous folding, docking and refinement of peptides onto their receptors. *PLoS One* 6(e18934):1–10.
81. Pfeiffer S, Fushman D, Cowburn D (2001) Simulated and NMR-derived backbone dynamics of a protein with significant flexibility: A comparison of spectral densities for the betaARK1 PH domain. *J Am Chem Soc* 123(13):3021–3036.
82. Pfeiffer S, Fushman D, Cowburn D (1999) Impact of Cl^- and Na^+ ions on simulated structure and dynamics of betaARK1 PH domain. *Proteins* 35(2):206–217.
83. Case D, et al. (2012) AMBER 13. University of California, San Francisco.
84. Le Grand S, Götz AW, Walker RC (2013) SPFP: Speed without compromise—A mixed precision model for GPU accelerated molecular dynamics simulations. *Comput Phys Commun* 184(2):374–380.
85. Shaw DE, et al. (2009) Millisecond-scale molecular dynamics simulations on Anton. Proceedings of the Conference on High Performance Computing Networking, Storage and Analysis (ACM, Portland, OR), pp 1-11.
86. Phillips JC, et al. (2005) Scalable molecular dynamics with NAMD. *J Comput Chem* 26(16):1781–1802.
87. Tribello GA, Bonomi M, Branduardi D, Camilloni C, Bussi G (2014) PLUMED 2: New feathers for an old bird. *Comput Phys Commun* 185(2):604–613.
88. Frishman D, Argos P (1995) Knowledge-based protein secondary structure assignment. *Proteins* 23(4):566–579.

Downloaded by guest on February 24, 2022